Photoionization of the scandium atom. III. Experimental and theoretical spectra from an excited state

D. J. Armstrong and F. Robicheaux*

Department of Physics and The Joint Institute for Laboratory Astrophysics, University of Colorado, Boulder, Colorado 80309-0440

We have carried out a relative measurement of the photoionization cross section of the excited Sc $(3d^3)^2_3 D_{3/2}$ state which lies 36 276.63 cm^{-1} above the ground state. These experimental results are compared with a calculated photoionization cross section. The theoretical cross section was obtained from scattering parameters and dipole matrix elements that were calculated prior to completion of the experiment and were not adjusted after we obtained the experimental data. The calculated cross section thus demonstrates the predictive power of this theoretical method. The observed features are accurately reproduced in a complicated region of the Sc autoionizing spectrum where numerous interacting channels converge to their respective ionization thresholds.

I. INTRODUCTION

In the two preceding papers [1,2], theoretical cross sections for photoionization of the Sc ground state have been compared with the photoabsorption data of Garton *et al.* [3]. The overall agreement with the available data has been quite good, and classifications were obtained for many previously unclassified lines in the Sc autoionizing spectrum. However, agreement between theory and experiment has so far been verified primarily by a comparison of the locations and relative strengths of only those lines which are easily identified in this earlier photographic plate data. Furthermore, classification of the Sc autoionizing spectrum has at times been ambiguous based on these data, due to simultaneous photoionization from the two lowest bound states. The Sc $(3d4s^2)^2 D_{3/2}$ ground state and the first excited $(3d4s^2)^2 D_{5/2}$ state are fine structure split by only 168.34 cm^{-1} [4]. The contribution from the $J = 5/2$ level arises due to the high ($\sim 2000\,^\circ$C) temperatures used in these ground-state measurements; the Boltzmann factor gives rise to nearly equal populations in these two lowest lying states. To overcome these complications, and to further test the R-matrix eigenchannel methods developed for Sc ground-state photoionization, we have completed extensive new measurements of the Sc photoionization spectrum from an excited state. These new excited state data provide a measurement which, within experimental constraints, faithfully reproduces the positions and line shapes of levels attached to the numerous interacting channels converging to the higher lying Sc ionization thresholds.

Selective excitation and photoionization of an excited state, in this case the Sc $(3d^3)^2_3 D_{3/2}$ state 36 276.63 cm^{-1} above the ground state [4], provides a rich testing ground for theory. With little or no excitation of any structureless continuum, the measured cross section consists of mostly symmetric line shapes (high Fano q parameter) except for some of the broad intense perturbers. Elimi-

nation of the additional photoionization signal from the $J = 5/2$ state combined with excitation of mostly high-l final states leads to a spectrum that is generally easy to interpret. Due to the inherently simple spectrum resulting from this experimental approach, we were able to verify many of the classifications of Garton *et al.* [3], and identify many previously unobserved lines in the Sc autoionizing spectrum.

This experiment utilized simple, relatively low resolution lasers, and was performed after modest low cost modifications to an existing apparatus. This measurement provided data over a broad spectal region covering seven ionization thresholds for a global test of theory, yet the resolution was high enough for line-by-line comparisons. There have apparently been few published measurements of excited state photoionization in other transition metals, but we hope the present measurements may open the door to further study. Since theoretical treatment of more complicated transition metals appears now to be within reach, the results presented here should encourage more experimental efforts. While the transition metals pose some technical difficulties (e.g., low vapor pressures and reactive vapor and liquid phases), the inherent simplicity of this experiment indicates that most of these difficulties can be easily overcome.

The calculation was described in more detail in the first paper of this series [1]. The theoretical cross sections were obtained from relatively small scale calculations on a work station; these calculations are nearly *ab initio* since the argonlike core electrons were incorporated through a model potential that gave a good fit to the Sc^{2+} energy levels. The short-range scattering parameters and dipole matrix elements were obtained before the experimental ion signal was measured; the theoretical spectrum constitutes a prediction for this process which the later measurements have confirmed. This bodes well for future studies of the heavier transition metals since these elements should present only slightly greater experimen-

tal difficulties than Sc.

This series of papers concentrated on photoionization near threshold. The theoretical methods used in this study are not limited to photoabsorption but can also be directly applied to low-energy electron-Sc$^+$ elastic and inelastic scattering; the experiment reported here tests the calculation at a much higher level than in an e-Sc$^+$ experiment due to the comparatively high resolution and better calibration of a photoionization experiment. Also, the calculated dipole matrix elements typically have larger errors than the calculated scattering parameters (e.g., the S matrix). The only difference is that photoionization restricts the final state to one parity and three different angular momenta for the final state whereas in e-Sc$^+$ the scattering parameters for both parities and all angular momenta are needed for the cross section.

In this paper we begin with a discussion of the experimental methods used to measure the Sc photoionization spectrum. The experimental and theoretical results are then presented in graphical form for easy comparisons. We give a table of newly observed lines with their classifications from theory and discuss some of the departures from simple Rydberg series with nearly constant quantum defects. We also compare the cross sections from the ground state and an excited state; the comparison illustrates how the different initial states emphasize different autoionizing states and changes the relative importance of the continuum versus resonant absorption.

II. EXPERIMENTAL METHODS

Many of the experimental methods in this work were similar to those used in a recent measurement of the Ba $(5d6p)^3D_1$ state photoionization cross section [5]. Some discussion of experimental details can be found in Ref. [5]. The relative measurement of the Sc photoionization cross section was performed by resonant two-step excitation and subsequent ionization of the Sc $(3d^3)_3^2D_{3/2}$ state. Details concerning ion collection and general data acquisition are discussed in Ref. [5]. Three Littman-type pulsed dye lasers excited and ionized Sc atoms in a thermal atomic beam. The lasers were pumped by the second and third harmonics of a Nd:YAG laser at a 10 Hz repetition rate. All three lasers had linewidths of ~ 0.5 cm^{-1} and pulse durations of 5–7 ns. No amplifiers were used with any of the lasers. The first laser was tuned into resonance with the transition from the $(3d4s^2)^2D_{3/2}$ ground state to the $(4s^24p)^2P_{1/2}^o$ excited state at $\lambda_1 = 534.4$ nm. The second laser was tuned into resonance with the transition from the $^2P_{1/2}^o$ state to the $(3d^3)_3^2D_{3/2}$ state at $\lambda_2 = 569.3$ nm, 36 276.63 cm^{-1} above the ground state. The third (scanning) laser was tuned continuously from $\lambda_3 = 601$ nm to 459 nm to measure the $(3d^3)_3^2D_{3/2}$ photoionization cross section over the energy range from the Sc$^+$ $(3d4s)^3D_1$ threshold to approximately 140 cm^{-1} above the $(3d^2)^3F_4$ threshold. Six different dyes were used in the scanning laser to cover this energy range of approximately 0.63 eV (5100 cm^{-1}). The spacing between data points, in terms of the scanning laser frequency, was approximately 2–3 GHz for the

measured spectrum.

All three lasers were linearly polarized and all polarization vectors were set parallel to each other. In the experiment it was convenient to use the excitation scheme $J = 3/2 \rightarrow J = 1^o/2 \rightarrow J = 3/2 \rightarrow J = 1^o/2$, $3^o/2$, $5^o/2$ final autoionizing states. This pathway only excites the $M = \pm 1/2$ final states if all of the excitations occur simultaneously with laser pulse durations which are short compared to time scales associated with any unresolved structure (e.g., hyperfine). However, the final bound state in this experiment was not expected to be strongly aligned due to the hyperfine interaction in Sc. This causes the precession of $\mathbf{J}$ for the $(3d^3)_3^2D_{3/2}$ state on nanosecond time scales (estimated from the hyperfine splittings of several Sc$^+$ states); since $\mathbf{J}$ probably precesses at least once during the ionizing pulse, there should be a net depolarization of the $(3d^3)_3^2D_{3/2}$ intermediate state and therefore the final states should not be polarized.

To reduce unwanted background ionization, the pulses from the second and third lasers were coincident in time and were optically delayed by 8 ns with respect to the first laser pulse. Since λ_1 could ionize the $(3d^3)_3^2D_{3/2}$ state excited by λ_2, this delay eliminated ionization by λ_1. In addition, the delay reduced any unwanted ionization signals which could arise when the scanning laser came into resonance with transitions from the $(4s^24p)^2P_{1/2}^o$ state to other bound states, including the $(3d^3)_3^2D_{3/2}$ state. The energy of λ_3 was always too small to directly ionize the $(4s^24p)^2P_{1/2}^o$ state. Since λ_2 had sufficient energy to ionize the $(3d^3)_3^2D_{3/2}$ state, there was a small constant background signal due to ionization of the $(3d^3)_3^2D_{3/2}$ state by λ_2. We did not find any evidence of resonance features in the measured cross sections caused by sources of unwanted photoionization.

At the point where the lasers intersected the Sc atomic beam, the spot sizes were approximately 0.02 cm^2 measured at the $1/e^2$ points. Tighter focus of the lasers was unnecessary as laser intensity requirements were quite modest. The transverse structure of the beams was not TEM$_{00}$, so measured pulse energies could provide only an estimate of laser intensity. The pulse energies of the first and second lasers were adjusted to ~ 2–4 μJ. These pulse energies provided an adequate excited state population, yet reduced unwanted background ionization of the $(3d^3)_3^2D_{3/2}$ state by the second laser to an acceptable level (less than a few percent of the total ion signal at a typical large resonance). The pulse energy of the ionizing (scanning) laser was set to a maximum of 15 μJ at the peak of the dye efficiency curve for each scan. With this pulse energy, there was probably some apparent broadening due to depletion of the final bound $(3d^3)_3^2D_{3/2}$ state for the stronger resonances [6,7]. To investigate this effect, we repeatedly scanned across the $(3d^2)^3F_2 15f$ state at $\lambda_3 = 477$ nm (a state whose width exceeds the laser linewidth) with successively lower pulse energies. For a pulse energy of 15 μJ, we observed very little (less than a few percent) depletion broadening when compared to the approximately constant observed width at lower pulse energies. While depletion of the final bound state is always an important consideration with autoionizing resonances

due to their large photoionization cross sections, many of the narrower resonances (e.g., members of a Rydberg series converging to a threshold) were broadened predominantly by the 0.5 cm^{-1} linewidth of the scanning laser. All of the measured spectra were normalized with respect to the scanning laser intensity, although as discussed in Ref. [5], this method of normalizing the data does not correct for the effect of depletion broadening.

We calibrated the wavelength of the scanning laser to an accuracy of approximately 1 cm^{-1} (approx. twice the scanning laser linewidth) for an accurate comparison with the earlier ground-state photoabsorption work of Garton et al. [3] and to extend classification of the odd parity Sc autoionizing spectrum. To do so, we first roughly calibrated λ_3 by recording the wavelength at the beginning of each data run with a monochromator with absolute accuracy of ±0.05 nm. The wavelength at any other data points was then determined relative to the first data point from the fringe signal of an étalon with a 101 GHz free spectral range. After the entire measured spectrum was calibrated in this manner, we examined the data runs with $\lambda_3 > 500$ nm and selected small energy ranges near the beginning and end of these runs which contained strong resonances. We then simultaneously recorded the Sc$^+$ signal and the absorption signal from a cell of iodine vapor over a short range of wavelengths near these resonances. The 0.5 cm^{-1} (15 GHz) linewidth of the scanning laser could not resolve the complicated iodine spectrum since the absorption linewidths in iodine vapor at room temperature are typically only 1.5 GHz. Nonetheless, locations of the strong resonances were determined with sufficient accuracy by comparing our measured iodine spectra with known spectra [8] which were convolved with a Gaussian weight function to account for the laser linewidth. The experimental data were then recalibrated after λ_3 had been determined more accurately for the strong resonances. An example of a convolved iodine spectrum and the measured iodine spectrum near the $(3d^2)^3F_47f$ resonance is shown in Fig. 1.

For wavelengths shorter than 500 nm where iodine vapor absorbs weakly, we improved on the monochromator calibration of λ_3 from a combination of previously classified Sc autoionizing lines [3] and comparison with the calculated cross section. The last method is quite reliable for high principal quantum number [e.g., near the $(3d^2)^3F_{2,3,4}$ thresholds where 468 nm $> \lambda_3 > 463$ nm] since experimentally derived threshold values are used in the calculations, and in this experiment mostly f-wave resonances are excited; these resonances typically have errors in the calculated quantum defects of < 0.02 which give errors less than 1 cm^{-1} for $n > 15$. Unfortunately, identification of previously classified lines can prove difficult for some parts of the spectrum where $\lambda_3 < 500$ nm because there were few identified $^3F_{J_c}nf$ lines in this energy range. In addition, there were few bound states accessible by λ_3 [i.e., other than the $(4s^24p)^2P^o_{1/2}$ and $(3d^3)^2_3D_{3/2}$] which could have conveniently provided frequency markers for calibration in the form of background photoionization signals. Furthermore, other sources of absorption spectra used to calibrate wavelengths below 500 nm (e.g., tellurium vapor) were not readily accessi-
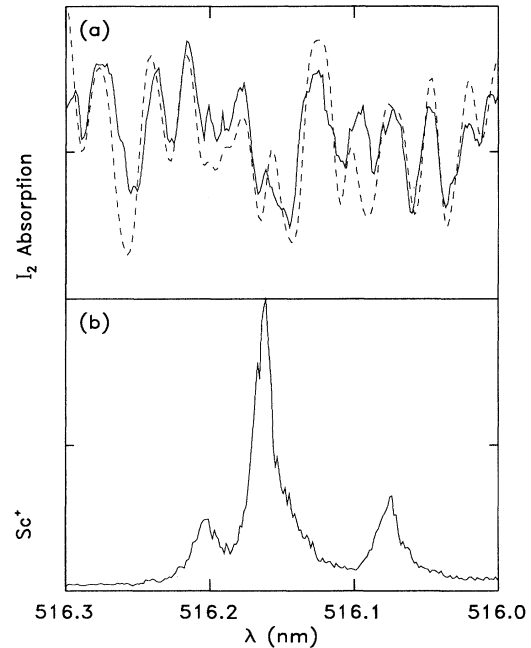

FIG. 1. (a) Convolved (dashed) and measured (solid) iodine spectrum. (b) Sc$^+$ signal near the $(3d^2)^3F_47f$ states.

ble. Consequently, energy calibration for some portions of the measured spectrum where $\lambda_3 < 500$ nm may be less accurate than 1 cm^{-1}.

The thermal beam of Sc atoms was produced by a resistively heated oven held at a constant temperature of approximately 1350 °C. An optical pyrometer was used to observe the temperature of the oven nozzle so that the temperature of the oven body itself, where the Sc was contained, was not well known. Disassembly of the oven after completion of the experiment revealed that the nozzle temperature was lower than the oven body temperature; the Sc metal had condensed on the inside surface of the oven surrounding the nozzle. The remaining Sc in the oven body had not melted, so the temperature of the oven itself was below the melting point of Sc at 1539 °C.

The oven was housed in the lower portion of a differentially pumped vacuum chamber. The ion collection apparatus, adjacent to the point where the lasers intersected the Sc beam, was housed in the upper portion of the chamber and was well isolated from the oven. For 1350 °C, the Sc vapor pressure in the oven would have been $\sim 5 \times 10^{-3}$ Torr [9], resulting in an estimated density of $\sim 3 \times 10^9$/cm^3 at the point of intersection with the three lasers in the upper chamber. The atom density can be estimated only roughly, owing to our poor knowledge of the oven temperature. The background pressure was $\sim 2 \times 10^{-7}$ Torr ($\sim 7 \times 10^9$/cm^3) in the upper portion of the vacuum chamber.

Several attempts with different ovens were required to reliably produce a thermal beam of Sc atoms adequate for these photoionization measurements. The relatively high temperature posed some problems for a resistively

heated oven. However, a design incorporating low thermal mass and low radiative losses was capable of maintaining 1350 °C. A more serious problem was determining the proper material for the oven itself, as most transition metals, including Sc, have highly reactive vapor and liquid phases. Earlier attempts with an oven made from molybdenum proved unsuccessful as an adequate beam was achieved only briefly when the oven was heated well above the Sc melting point and molten Sc escaped from the oven forming a dense cloud of Sc vapor in the lower vacuum chamber. For temperatures below the Sc melting point, the reaction between Sc and molybdenum was apparently strong enough to hinder generation of an atomic beam. At temperatures above the Sc melting point in high vacuum, Sc vapor reacted with the molybdenum and formed a strong braze weld between the oven parts. Following the photoabsorption work of Tomkins and Ercoli and Garton et al. [10,3] where a furnace lined with tantalum was used with Sc at temperatures up to 2200 °C, we constructed an oven from tantalum and found it worked well for temperatures below the Sc melting point. There was some evidence that Sc reacted with tantalum at these temperatures but not to an extent that prevented generation of a thermal atomic beam.

The oven used in this experiment was machined from solid tantalum to form a cylinder of 2.1 in. length with 0.8 in. outside diameter and 0.44 in. inside diameter. The two pieces of the cylinder, the lower oven body, and the upper part with a 0.040 in. diameter nozzle were joined by a 4° taper fit. A 1.0 in. outside diameter alumina insulator wrapped with 16 turns of 0.009 in. diameter tungsten wire surrounded the oven and served as the heating element. The oven was mounted such that losses due to heat conduction were minimal, and the oven assembly was surrounded by four concentric cylindrical heat shields with caps top and bottom to reduce radiative losses. The two inner shields were made from tantalum, while the outer shields were made from stainless steel. The entire oven-plus-radiation-shield assembly was then surrounded by (but not in contact with) a water-cooled copper cylinder to reduce heating of the vacuum chamber.

A variable autotransformer was used to supply current to the tungsten heating coil. To maintain a nozzle temperature of 1350 °C, typical operating current was 4.3 A at 90 V. The tungsten heating element survived for the duration of this experiment (∼ 100 h), but a more reliable design intended for long-term use would probably incorporate electron beam heating or inductive heating.

III. THEORETICAL METHODS

We used the same theoretical techniques as those described in the previous papers [11]. See Ref. [1] for a discussion of the choice of basis functions used in this calculation. The only difference between the calculations described in Ref. [1] and the current calculations is the initial state; in this calculation it is the $(3d^3)_3^2 D_{3/2}$ state at $36\,276.63$ cm^{-1} above the ground state. We utilized the same principles as Ref. [1] for choosing the basis functions to achieve convergence of the initial state. We used an initial state that has the same L, S, and J as the ground state in order to probe the same final states as Garton et al. [3]; the different initial states emphasize different resonance structures in the photoionization process which should give a different perspective of the Sc dynamics.

As in previous work, the streamlined version of the eigenchannel R-matrix technology [12] was used to obtain the scattering parameters and dipole matrix elements in LS coupling. (We used basis functions that incorporated configuration interaction in both the $N-1$-electron ionic states and the full N-electron wave function.) These parameters were obtained on a coarse mesh then interpolated to obtain them on the fine mesh used to calculate the cross section. We then utilized the LS to jj frame transformation [13] to incorporate the spin-orbit splittings of the core. The boundary conditions at $r \to \infty$ were enforced using standard formulas of multichannel quantum defect theory (MQDT) [14]. The calculated cross section was obtained at 200 000 energies for the whole range of Figs. 2–5. There are numerous very narrow resonances that would be missed with a smaller mesh. The total calculation for the length and velocity gauge cross sections for $3/2 \to 1^o/2$, $3^o/2$, $5^o/2$ was less than 10 CPU hours on a DEC 5240 work station computer.

In the calculation, we used multichannel quantum defect theory to obtain the theoretical cross section. However, in discussing the properties of the resonances we will only use single-channel quantum defect theory. The important parameter is the quantum defect, μ, which is the phase shift (divided by π) of the Sc wave function compared to the hydrogenic function; the quantum defect appears in the resonance energy through $E_n = E_c - 1/2(n - \mu)^2$ where E_c is the energy of the core electrons in atomic units. The effective quantum number, $\nu \equiv n - \mu$, is proportional to the "number" of
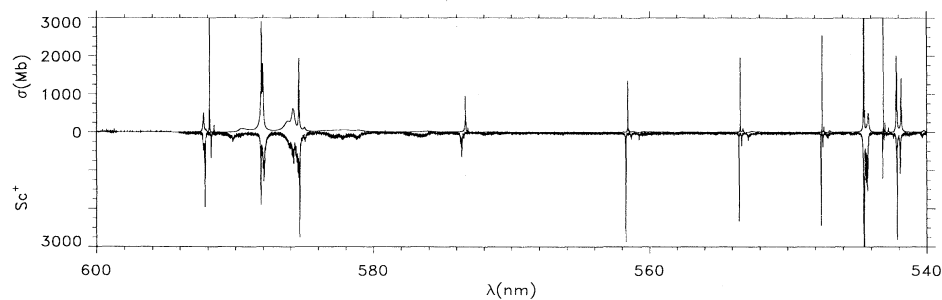

FIG. 2. The experimental ion signal (lower curve) and the length gauge theoretical cross section (unconvolved upper curve) as a function of the wavelength of the third laser.
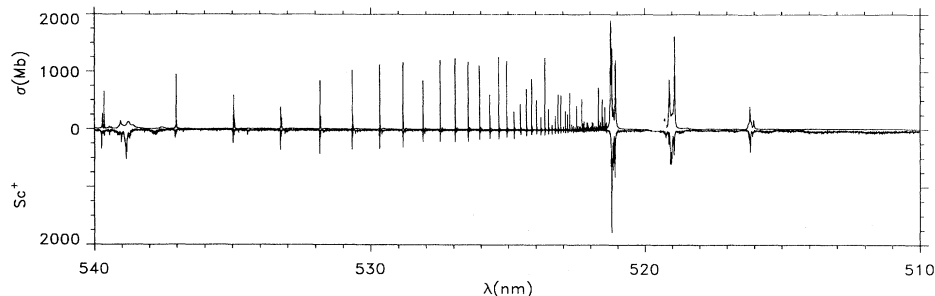
FIG. 3. Same as Fig. 2. Note change of wavelength scale.

radial nodes, $n_r = \nu - \ell - 1$, that a hydrogenic wave function would have at energy $-1/2\nu^2$. Because μ is proportional to the phase shift, the derivative of μ with respect to energy is proportional to the time delay of an electron scattering from the Sc^+ compared to the time delay of an electron scattering from a proton; this relative time delay is small since the electron-Sc^+ interaction only differs from the e-proton interaction at short distances where the electron is moving fastest. Our estimate of $d\mu/dE$ is $\sim 0.04/eV$. This estimate holds only when there are no perturbing states because the electron can be trapped into the perturbing state for relatively large times which implies a larger time delay and therefore a larger energy dependence in the quantum defect.

IV. RESULTS

A. Experimental and theoretical spectra

In Figs. 2–5, we show the unconvolved theoretical cross section [from the $(3d^3)^2_3 D_{3/2}$ excited state $36\,276.63$ cm^{-1} above the ground state [4]] and the measured Sc^+ signal as a function of the scanning laser wavelength. As discussed in the experimental section, the ion signal for each separate data run was first normalized with respect to the scanning laser intensity. The measured cross sections were then normalized once again with respect to each other to achieve the most accurate comparison with the calculated cross sections. The relative normalization of the Sc^+ signal for each run was obtained by comparing the height of resonances that appeared in data runs that overlapped in wavelength. When adjacent data runs had no resonances in common, fluctuations in the baseline signal were used as a rough guide for the normalization. The Sc^+ signal was then matched to the theoretical size

of the moderately broad and intense ^3F5f and ^3F7f resonances near $\lambda_3 = 587$ and 520 nm, respectively. These resonances were selected as a starting point since theory and experiment should agree the best at broad features where laser linewidth and saturation effects (e.g., depletion broadening) should be smallest. Although experiment and theory were brought into agreement in one small region, and normalization of the Sc^+ signal was carried on from that region, the measured cross section is strictly relative. The numbers associated with the experimental Sc^+ signal in Figs. 2–5 are intended only for comparison and do not imply an absolute measurement.

Although better agreement with experiment can be achieved by convolution of the theoretical spectrum with the laser linewidth, the spectrum in Figs. 2-5 was not convolved. The energy mesh of the calculated cross section was too coarse to completely trace the narrow high-n resonances; the calculation used $200\,000$ energy mesh points from threshold to $\lambda \sim 460$ nm but would (probably) have needed more than a million points to do an adequate job. Because the calculated spectrum was unconvolved, the high-n resonances are much more intense than in the experimental spectrum. As an example of the good agreement that can be achieved with convolution, Fig. 6 shows a small portion of the cross section from $\lambda_3 = 468$–467 nm that was calculated with $10\,000$ energy mesh points per nm. Subsequent convolution with a Gaussian line profile of 0.4 cm^{-1} brought the theoretical line shapes into excellent agreement with the measured line shapes (the experimental profiles may be slightly narrower). This spectral region was chosen randomly to show the interacting Rydberg series attached to the three ^3F thresholds; we subsequently compared unconvolved theoretical spectra to the experimental spectra and found excellent agreement in resonance positions except near the $(4s^24f)^2F^o_{5/2}$ resonance where the agree-
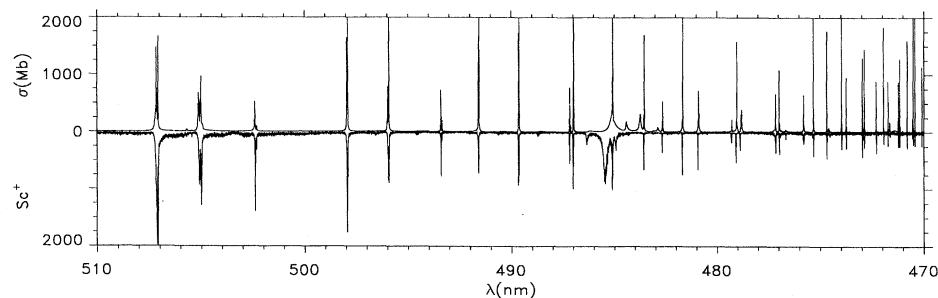

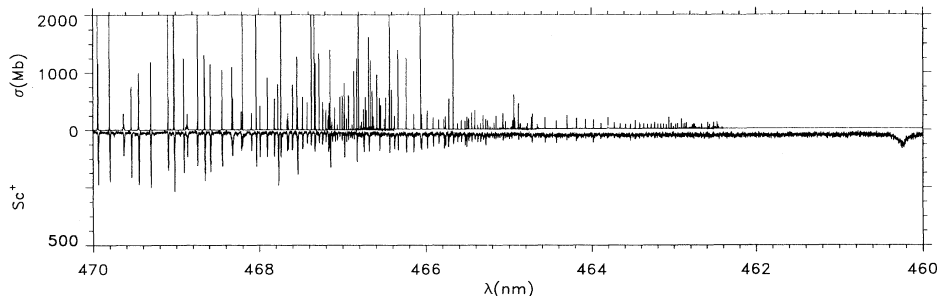FIG. 4. Same as Fig. 2. Note change of wavelength scale.

FIG. 5. Same as Fig. 2. Note change of wavelength scale. Also note change of scale for the measured cross section. This exaggerates the height of the measured baseline, and enhances visibility of the experimentally observed broad resonance at $\lambda_3 = 460.25$ nm.

ment was still good but not at the same level as Fig. 6. All of the resonances are f-wave resonances attached to the $^3F_{J_c}$ thresholds. The ^3F_2nf ($n \sim 44$ near the middle of the figure) series is perturbed six times by ^3F_3nf and ^3F_4nf states: (1) the $^3F_3(27–30)f$ states are near 467.77 nm, 467.54 nm, 467.34 nm, and 467.14 nm; (2) the $^3F_4(21,22)nf$ states are near 467.66 nm and 467.17 nm. The $^3F_243f$ states and the $^3F_328f$ states near 467.54 nm are unresolved by the experiment. The interactions between the states of different series are relatively small. This interaction as well as the size and positions of the peaks have been accurately reproduced by the calculation. We do not have a simple explanation for why the oscillator strength to the ^3F_4nf states is so much smaller than to the states of the ^3F_3nf series; the ^3F_2nf states have a smaller oscillator strength due to the $1/n^3$ factor in the square of the dipole matrix element; n is much larger for the ^3F_2nf states than for the ^3F_3nf states in this figure.

The measurement of the Sc $(3d^3)^2_3D_{3/2}$ state photoionization cross section began at $\lambda_3 = 601$ nm to include the first three Sc$^+$ $(3d4s)^3D_{1,2,3}$ ionization thresholds at $\lambda_3 = 600.7$, 598.3, and 594.4 nm. However, since the amplitude to excite the various channels converging to these thresholds from the $(3d^3)^2_3D_{3/2}$ state is so weak, this portion of the spectrum is nearly devoid of any features for the experiment and the theory. Due to an essentially featureless cross section, the region for $\lambda_3 > 600$ nm was omitted from Fig. 2. Any structure in the measured cross section near these thresholds was indistinguishable from statistical fluctuations (i.e., noise) in the baseline of the Sc$^+$ signal. For the rest of the measured cross section seen in Figs. 2–5, the baseline is characterized by noise in the Sc$^+$ signal and it is usually somewhat elevated when compared to the calculated cross section. The noise in the baseline is simply due to shot-to-shot fluctuations in the intensity of the three pulsed dye lasers. The slightly elevated baseline arises from a small but constant background ionization signal due to λ_2. It was fortuitous that the region of the photoionization cross section near λ_2 contained no strong resonances.

The agreement between the measured and calculated cross sections in Figs. 2–5 is overall quite good. For example, in the region that contains the $^3F_{2,3,4}$ thresholds in Fig. 5, the positions of the resonances that belong to the various perturbed Rydberg series line up nearly exactly. As discussed in the experimental section, this is not an unanticipated result as the experimental thresh-

old values are used in the calculation. Furthermore, a few of the high n resonances have been used for calibration of λ_3. However, that calibration procedure ensures good agreement between theory and experiment for only a few of the resonances. The good agreement seen in Fig. 5 is primarily due to an accurate determination of the quantum defects for the various interacting channels.

Similar good agreement is seen for the Rydberg series converging to the $(3d4s)^1D$ threshold at $\lambda_3 = 521.2$ nm in Fig. 3. However, on close inspection one sees a small disagreement in location between experiment and theory for the low n members of this series. For even longer wavelengths (i.e., lower n) in Fig. 2, the disagreement becomes more pronounced as errors in the calculated quantum defects, which are fairly energy independent, are no longer negligible compared to n. For example, the ^1D8f resonances near $\lambda_3 = 573.6$ nm in Fig. 2 have an error in the calculated quantum defects of $0.01 - 0.02$ when compared to the experiment. Errors of this size are typical for this type of calculations (see the previous work in the alkaline earths [5]).

In the region of the spectrum shown in Fig. 4 near $\lambda_3 = 485$ nm, we see the $(3d^2)^1D4f$ states, broad perturbers whose energies are not reproduced well by the calculation. An example such as the $(3d^2)^1D4f$ states is not unexpected in calculations of this type. As discussed in Sec. III, errors in the calculated quantum defect will always be more pronounced for any resonance with low n. The error in the calculated quantum defects of these states is ~ 0.01. The cross section can look very different when the perturber is not at the exact energy due to interferences between the amplitudes for photoexciting the
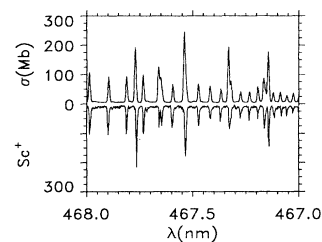

FIG. 6. Same as Fig. 2 but with the theoretical cross section convolved with a Gaussian weight function of 0.4 cm^{-1} full width at half maximum. At 467.5 nm the effective quantum number, $\nu = [2(E_c - E)]^{-1/2}$, is 21.3 in the $^3F_4$ channels, 28.1 in the $^3F_3$ channels, and 43.5 in the $^3F_2$ channels.
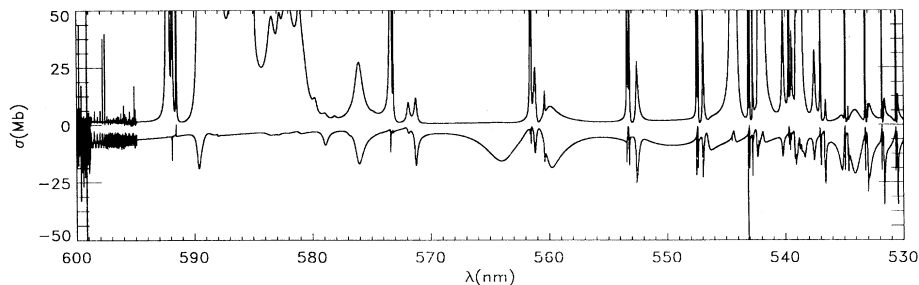
FIG. 7. Calculated photo-ionization cross sections from the ground state and from the $(3d^3)^2_3 D_{3/2}$ excited state 36 276.63 cm^{-1} above the ground state. The upper curve is the excited state cross section.

perturber and the amplitudes for photoexciting the states that it perturbs. That the $(3d^2)^1 D 4f$ resonances are the most prominent example in this cross section is probably due to the small n and the expanded wavelength scale that is used for the graph; the $5f$ resonances have half the error in their energy that the $4f$ resonances do when the error in the quantum defects is the same. The only other example of truly conspicuous disagreement is the absence of the broad resonance at $\lambda_3 = 460.25$ nm from the calculated cross section near the right edge of Fig. 5. However, the difference in scale from the theoretical and experimental results in Fig. 5 should be noted. There are two $(3d^2)^3 P 4f$ resonances in the calculation at this energy (one with a quantum defect error of ~ 0.005 and the other with a quantum defect error of ~ 0.013) but they each have a factor of ~ 2 less oscillator strength than in the experiment. It is possible that the experimental line is made up of the sum of these two lines in which case there would be no disagreement.

B. Comparison of theoretical cross sections from the ground and excited state

In Figs. 7 and 8 we show the photoionization cross section from the $(4s^2 3d)^2 D_{3/2}$ ground state and the $(3d^3)^2_3 D_{3/2}$ excited state at 36 276.63 cm^{-1} above the ground state [4]; the range is from threshold to just above the $(3d^2)^3 F$ thresholds. The wavelength is for photoionization from the excited state; the cross section for photoionization from the ground state is plotted so that the energy of the final state is 36 276.63 cm^{-1}+$1/\lambda$ and therefore the resonance positions for the different cross sections match. As expected the cross section differs greatly for the two different initial states.

The difference between the different cross sections can

help in the classification of resonances. As an example, we expand the wavelength region near the $(4s3d)^1 D 7f$ states in Fig. 9 showing the calculated cross sections from the $(3d^3)^2_3 D_{3/2}$ and from the ground state. We have classified the central peak as $^1 D 7f^2 F^o_{5/2}$ (at 592.19 nm in the experiment), the lower energy peak as $^1 D 7f^2 D^o_{3/2}$ (at 592.28 nm in the experiment), and the higher energy peak as $^1 D 7f^2 P^o_{1/2}$ (at 591.73 nm in the experiment). This cross section clearly shows the *qualitative* difference when photoionizing the $(3d^3)^2_3 D_{3/2}$ state versus the ground state. From the excited state all of the resonances are peaks whereas from the ground state the leftmost resonance does not appear in the cross section, the rightmost resonance has a window profile, and the central resonance (the only feature observed by Garton et al. [3]) is a Lorentzian peak. The difference between the experimental and theoretical positions is larger than spacings of the resonances; in the experiment the splitting of the $^2 D^o_{3/2}$ and $^2 F^o_{5/2}$ resonances is 0.09 nm which makes the classifications of the experimental lines problematical. However, as is clear from the figure only the $^2 F^o_{5/2}$ line should have been (and was) observed in the experiment of Garton et al. [3] at an energy that would correspond to $\lambda = 592.20$ nm; their line unambiguously matches our experimental line at 592.19 nm which enables a solid classification of the 592.19 nm line. The remaining two lines have a large enough spacing to permit a definite classification. Another example is the $^3 F n f$-wave resonances between 510 and 490 nm. In the experiment of Garton et al. these appear as sharp window resonances and resonances with asymmetric Fano profiles whereas in the current experiment they appear as extremely tall Lorentzian peaks.

The comparison between the two experiments only changed the classification of one resonance from the orig-
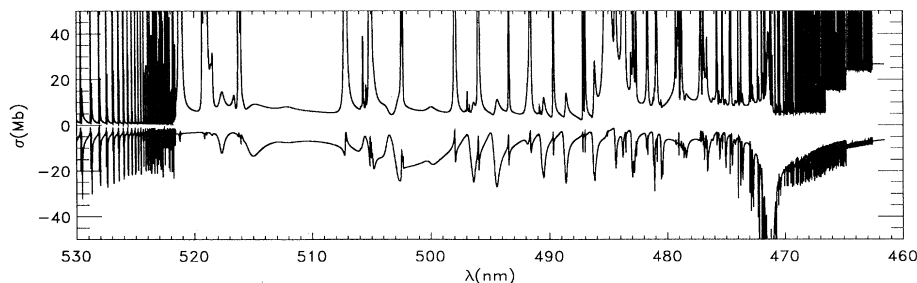

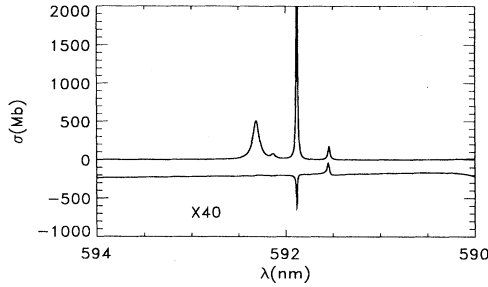FIG. 8. Same as Fig. 7 except different wavelength range.

FIG. 9. Same as Fig. 7 except different wavelength range.

inal classifications using the data of Garton et al. and the theoretical cross sections from the ground state [2]. This was the $^1D9f^2F^o_{5/2}$ line; we originally classified this line as $^2P^o_{1/2}$ because in photoionization from the ground state the theoretical $^2P^o$ line was more intense than the $^2F^o$ line although the theoretical position of the $^2F^o$ line was closer to the experimental energy. Probably, the $^3P5p^2P^o$ perturber which can be clearly seen in Fig. 7 of Ref. [1] was slightly lower than its calculated energy. This state broadens the $^1D(10$–$30)f^2P^o$ and if it were slightly lower in energy (which would not be surprising because its $\nu \sim 3$ is so small) it would also broaden the $^1D9f^2P^o$ state; this would lower its peak cross section making the $^2F^o$ state more noticeable.

The photoionization cross section appears different for different initial states because the dipole matrix element that couples the initial and final state depends on both the initial *and* final state. This is a point that cannot be emphasized enough; the position and width of a resonance are intrinsic properties of the final state (and therefore will be the same for any initial state) but the shape and height of the resonance depend on the relative size and phase of the dipole coupling of the initial state to the resonance state and to the continuum.

The dipole operator is a one-electron operator and therefore can only change one orbital. Since the initial states consist of only $3d$ and $4s$ orbitals, we examined the one-electron matrix elements $\langle 3d||z||\varepsilon p\rangle$, $\langle 3d||z||\varepsilon f\rangle$, and $\langle 4s||z||\varepsilon p\rangle$ where $\varepsilon \sim 0$. We found that the amplitude for $3d \to \varepsilon f$ was ~ 2.5 times larger than the amplitude for $4s \to \varepsilon p$ and was ~ 4 times larger than the amplitude for $3d \to \varepsilon p$. This implies that the cross section from a $3d^3$ initial state will be dominated by f-wave resonances; from the ground state p-wave resonances can dominate. Since Sc is the first atom that incorporates a $3d$ electron in its ground state, it might be expected that the $3d \to \varepsilon f$ amplitude would be comparable to the $3d \to \varepsilon p$ amplitude (for the atoms B through Ne the $2p \to \varepsilon d$ amplitudes are comparable to the $2p \to \varepsilon s$ amplitudes). There are two differences between Sc and the first row atoms B–Ne. In H, the $3d \to nf$ oscillator strength is ~ 60 times bigger than the $3d \to np$ oscillator strength whereas the $2p \to nd$ oscillator strength is ~ 30 times bigger than the $2p \to ns$ oscillator strength which indicates $\ell \to \ell+1$ is more strongly favored for $\ell = 2$ than for $\ell = 1$. The $3d \to \varepsilon p$ dipole matrix element is reduced in Sc by the presence of a node in the εp orbital at the same

distance as the antinode of the $3d$ orbital (see Figs. 1 and 2 of Ref. [1]). We expect the major features of the cross section from the $3d^3$ state to be more accurate than those from the $4s^23d$ ground state because the calculated cross sections are more accurate for f-wave channels (because f waves do not penetrate as far into the complicated core region). The peaks are roughly two orders of magnitude larger for excitation from the $3d^3$ state than from the $4s^23d$ state except for excitations $4s^23d \to 4s^2nf$. One order of magnitude comes from the square of the $d \to f$ and $s \to p$ matrix elements (over a large range the main peaks from the ground state are $4s^23d \to 4s3dnp$); one order of magnitude comes from the difference in the widths of f- and p-wave resonances (i.e., the height of the cross section is proportional to D^2/Γ where D is the dipole matrix element to the resonant state and Γ is the resonance width).

The f-wave resonances from the $4s^23d$ state were very strong for the $4s^2nf$ series as expected; the other f-wave states arise because configuration interaction mixes some $3d^3$ into the $4s^23d$ state. The number of channels that can be probed by photoabsorption depends on the purity of the initial state; the more configuration interaction the greater the number of channels that can be excited.

C. Classifications and energies of experimental autoionizing lines

In Table I, we give the energies above the ground state and the classifications for the prominent resonances of this experiment; we only give the resonances for the dyes that were wavelength calibrated to the iodine spectrum. We also do not give the energies of the ^1Dnf and np states with $\nu > 21$ because the energies of these states can be obtained more accurately from $E_n = E_c - 1/2(n-\mu)^2$ where E_c is the ^1D threshold energy in atomic units and μ is the quantum defect which can be extrapolated from the $n - \nu$ of the lower levels. We have included the energies from Garton et al. [3] for lines that appear in both experiments. As stated in the previous paper [2], the compilation [4] of Sc levels averaged the energies of lines arising from different final states in the new classification [2] due to original misclassification of lines.

The classifications that we have marked with "?" indicate less confidence in the classification than for the other lines. The $^1D(15$–$17)p^2D^o_{3/2}$ lines were uncertain due to the proximity of perturbers in the calculation and the experiment. For most of the ^3Fnf states we could not determine the total angular momentum because of the near degeneracy of these states. To determine J, the relative errors in our calculated quantum defects would need to be less than 0.003. Also, some of the lines were probably the unresolved sum of two or more lines; there should be 5 ^3F_2nf lines, 6 ^3F_3nf lines, and 5 ^3F_4nf lines. (The $^3F_48f$ line at 56181.2 cm^{-1} may not be identical to the 56180.0 cm^{-1} line observed by Garton et al. [2,3] since there are obviously a large number of $^3F_48f$ lines that were not observed in either experiment.)

As discussed in the preceding section the quantum defect should remain roughly constant over a Rydberg se-

ries except near perturbers; of course, a jump in quantum defect could also indicate a misclassification of a level so we give the reasons for the energy dependences in some of the quantum defects. One of the more striking jumps is the change by 0.04 in the quantum defect going from the $^1D8f^2D^o_{3/2}$ to the $^1D9f^2D^o_{3/2}$ level. This jump is caused by the $^3F7p^2D^o_{3/2}$ level which is at a slightly lower energy than the $^1D9f^2D^o_{3/2}$ state and pushes it to higher energy (i.e., larger value of ν, smaller value of μ); the $^3P5p^2D^o_{3/2}$ state is also at slightly smaller energies and

is much broader than the $^3F7p^2D^o_{3/2}$ state. It can be seen in the experimental cross section (when the wavelength scale is expanded) that the $^1D9f^2D^o_{3/2}$ state is relatively broader than the $^1D10f^2D^o_{3/2}$ state which is relatively broader than the $^1D11f^2D^o_{3/2}$; the quantum defect increases from the $9f$ to the $12f$ state. These are the signs of interaction with the broad $^3P5p^2D^o_{3/2}$ perturber. The $^1D13f^2D^o_{3/2}$ is pushed to higher energies by the $^3F_28p\ J = 3^o/2$ perturber and the $^1D14f^2D^o_{3/2}$ and

TABLE I. Energy from ground state and classification of autoionizing states compared to those of Garton et al. when possible. The $(4s3d)^1D$ core state has been shortened to ^1D and the $(3d^2)^3F_{J_c}$ states have been shortened to $^3F_{J_c}$. The uncertainty in the energies is 1.0 cm^{-1}; we have given the wavelengths to the nearest Å for ease of finding the resonances on the figures. See text for explanation of questionable classifications.

λ_3(nm)	E(cm^{-1})[a]	E(cm^{-1})[b]	Classification	ν
591.7	53176.2		$^1D7f\ ^2P^o_{1/2}$	6.927
573.5	53714.3		$^1D8f\ ^2P^o_{1/2}$	7.922
592.3	53160.3		$^1D7f\ ^2D^o_{3/2}$	6.903
573.7	53707.3	53707.1	$^1D8f\ ^2D^o_{3/2}$	7.906
561.3	54091.6		$^1D9f\ ^2D^o_{3/2}$	8.945
553.3	54350.7		$^1D10f\ ^2D^o_{3/2}$	9.933
547.4	54543.9		$^1D11f\ ^2D^o_{3/2}$	10.927
543.0	54691.3		$^1D12f\ ^2D^o_{3/2}$	11.925
539.6	54807.3		$^1D13f\ ^2D^o_{3/2}$	12.937
537.0	54897.9		$^1D14f\ ^2D^o_{3/2}$	13.936
534.9	54970.5	54970.8	$^1D15f\ ^2D^o_{3/2}$	14.928
533.2	55030.3	55030.7	$^1D16f\ ^2D^o_{3/2}$	15.926
531.8	55080.0		$^1D17f\ ^2D^o_{3/2}$	16.928
530.6	55121.5		$^1D18f\ ^2D^o_{3/2}$	17.927
529.7	55156.7		$^1D19f\ ^2D^o_{3/2}$	18.93
528.8	55186.8		$^1D20f\ ^2D^o_{3/2}$	19.93
528.1	55212.5		$^1D21f\ ^2D^o_{3/2}$	20.93
592.2	53163.0	53162.7	$^1D7f\ ^2F^o_{5/2}$	6.907
573.6	53710.1		$^1D8f\ ^2F^o_{5/2}$	7.912
561.7	54079.0	54079.5	$^1D9f\ ^2F^o_{5/2}$	8.905
553.5	54343.6	54343.6	$^1D10f\ ^2F^o_{5/2}$	9.901
547.6	54539.1	54539.3	$^1D11f\ ^2F^o_{5/2}$	10.899
543.2	54687.4	54687.5	$^1D12f\ ^2F^o_{5/2}$	11.895
539.7	54803.8	54803.6	$^1D13f\ ^2F^o_{5/2}$	12.903
537.1	54896.4	54895.3	$^1D14f\ ^2F^o_{5/2}$	13.917
535.0	54969.1		$^1D15f\ ^2F^o_{5/2}$	14.907
533.3	55029.1		$^1D16f\ ^2F^o_{5/2}$	15.904
531.8	55079.0		$^1D17f\ ^2F^o_{5/2}$	16.906
530.7	55120.6		$^1D18f\ ^2F^o_{5/2}$	17.904
529.7	55155.8		$^1D19f\ ^2F^o_{5/2}$	18.90
528.8	55186.1		$^1D20f\ ^2F^o_{5/2}$	19.90
528.1	55211.9		$^1D21f\ ^2F^o_{5/2}$	20.90
547.2	54552.8	54553.4	$^1D9p\ ^2F^o_{5/2}$	10.980
560.7	54110.0		$^1D11p\ ^2F^o_{5/2}$	9.006
552.8	54366.0	54365.6	$^1D12p\ ^2D^o_{3/2}$	10.002
547.1	54556.0	54556.2	$^1D13p\ ^2D^o_{3/2}$	11.000
539.5	54813.7		$?^1D15p\ ^2D^o_{3/2}$	13.001
536.8	54906.1	54906.2	$?^1D16p\ ^2D^o_{3/2}$	14.038
534.4	54987.7		$?^1D17p\ ^2D^o_{3/2}$	15.196
533.0	55036.6	55036.4	$^1D18p\ ^2D^o_{3/2}$	16.043
531.7	55083.9	55084.2	$^1D19p\ ^2D^o_{3/2}$	17.015
530.6	55124.9	55125.0	$^1D20p\ ^2D^o_{3/2}$	18.017
529.6	55159.2	55159.2	$^1D21p\ ^2D^o_{3/2}$	19.01
528.8	55189.0		$^1D22p\ ^2D^o_{3/2}$	20.01
528.0	55214.4	55214.3	$^1D23p\ ^2D^o_{3/2}$	21.01
588.2	53279.0		$^3F_25f\ 5^o/2$	4.968
587.9	53285.5		$^3F_25f\ 3^o/2$	4.972
585.8	53347		$^3F_35f\ 3^o/2$	4.961
585.3	53360.7		$^3F_35f\ 5^o/2$	4.969
584.9	53373		$^3F_35f\ 1^o/2$	4.976
544.5	54642.1		$^3F_26f\ 5^o/2$	5.966
544.4	54646.8		$^3F_26f\ ?^o/2$	5.971
544.3	54650.2		$^3F_26f\ ?^o/2$	5.974
542.1	54722.4		$^3F_36f\ 5^o/2$	5.966
541.9	54730.3		$^3F_36f\ 3^o/2$	5.974
539.0	54828.6		$^3F_46f\ ?^o/2$	5.968
538.9	54834.5		$^3F_46f\ ?^o/2$	5.974
538.7	54838.9		$^3F_46f\ ?^o/2$	5.978
537.8	54871		$^3F_38p\ 5^o/2$	6.115
521.2	55462.3		$^3F_27f\ ?^o/2$	6.964
521.2	55462.7		$^3F_27f\ ?^o/2$	6.965
521.2	55464.6		$^3F_27f\ ?^o/2$	6.968
521.1	55466.9		$^3F_27f\ ?^o/2$	6.971
519.2	55535.9		$^3F_37f\ ?^o/2$	6.953
519.1	55539.9		$^3F_37f\ ?^o/2$	6.960
519.1	55542.2		$^3F_37f\ ?^o/2$	6.963
519.0	55543.5		$^3F_37f\ ?^o/2$	6.965
518.9	55546.9		$^3F_37f\ ?^o/2$	6.970
518.9	55547.4		$^3F_37f\ ?^o/2$	6.971
516.2	55649.0		$^3F_47f\ ?^o/2$	6.967
516.2	55650.5		$^3F_47f\ ?^o/2$	6.969
516.1	55654.0		$^3F_47f\ ?^o/2$	6.975
507.1	55995		$^3F_28f\ ?^o/2$	7.965
507.1	55996		$^3F_28f\ ?^o/2$	7.967
507.1	55997.5		$^3F_28f\ ?^o/2$	7.970
505.1	56074.9		$^3F_38f\ ?^o/2$	7.963
505.0	56077.4		$^3F_38f\ ?^o/2$	7.969
505.0	56078.3		$^3F_38f\ ?^o/2$	7.971
502.4	56181.2	56180.0	$^3F_48f\ ?^o/2$	7.968
502.3	56183.8		$^3F_48f\ ?^o/2$	7.974
497.9	56359.5	56359.7	$^3F_29f\ ?^o/2$	8.965
497.9	56360.6		$^3F_29f\ ?^o/2$	8.969

[a]Present results.
[b]Results of Garton et al.

$^1D14f\,^2F^o_{5/2}$ states are pushed to higher energies by the $^3F_38p\,J = 3^o/2$ and $5^o/2$ perturbers, respectively.

The ^3Fnf states are not perturbed in the energy range between the $5f$ and $9f$ states except for the $^3F_45f$ states. These states interact very strongly with the $^3P5p^4P$ and $^3F_27p$ perturbing states. These interacting states are near 582 nm; as can be seen in Fig. 2 the perturbers greatly broaden the $^3F_45f$ states which is why we have not reported their positions in Table I. The ^3Fnf series are seriously perturbed at higher energies. The most notable perturbers are the $(3d^2)^1D4f$ perturbers near 485 nm.

A final striking feature of the cross section was the disappearance of the $(4s3d)^1Dnf^2P^o_{1/2}$ resonances for $n \geq 9$. This can be explained by an examination of the cross section for photoionization from the ground state. The $J = 1^o/2$ cross section of Figs. 1 and 2 of Ref. [2] clearly shows an extremely broad perturber interacting with the $(4s3d)^1Dnf^2P^o_{1/2}$ resonances. The perturber is the $(3d^2)^3P5p^2P^o_{1/2}$ state which has a width of ~ 900 cm^{-1}. This perturber greatly increases the width of the ^1Dnf resonance states from $n = 10$–30. This reduces the peak heights of the ^1Dnf resonances which makes them difficult to detect (peak heights decrease like the inverse of the resonance width). In the calculation the $^1D9f^2P^o_{1/2}$ state is outside of the width of the ^3P5p state and is therefore not broadened by it. However, a small error in the calculated quantum defect of this perturbing state would result in a relatively large energy shift; therefore, it is believable that the $^1D9f^2P^o_{1/2}$ state actually falls within the width of the resonance; the estimated error in the theoretical energy of the $^3P5p^2P^o_{1/2}$ state is large enough that it could broaden the $^1D9f^2P^o_{1/2}$ resonance.

The $^3P5p^2P^o$ perturbing state does not affect the $(4s3d)^1Dnf^2P^o$ series in the manner that the $(3d^2)^3P5p^2D^o$ state affects the $(4s3d)^1Dnf^2D^o$ states. The $^1Dnf^2P^o$ states that interact with the ^3P5p perturber are broadened to the point of being undetectable by this experiment whereas the $^1Dnf^2D^o$ states are mostly shifted in energy. The reason for this difference is the $^3P5p^2P^o$ state is most strongly coupled to the $(4s3d)^3D\varepsilon p^2P^o$ continuum whereas the $^3P5p^2D^o$ level is most strongly coupled to the $(4s3d)^1Dnp^2D^o$ Rydberg series. For the $^2P^o$ symmetry the interactions give $^1Dnf \leftrightarrow\,^3P5p \rightarrow\,^3D\varepsilon p$ (i.e., by interacting with the perturber the $^1Dnf^2P^o$ states can decay quicker), and for the $^2D^o$ symmetry the interactions give $^1Dnf \leftrightarrow\,^3P5p \leftrightarrow\,^1Dnp$ (i.e., by interacting with the perturber, a secondary interaction with the ^1Dnp states is induced).

Table I shows that the quantum defects for the f waves attached to the $(3d^2)^3F$ thresholds are ~ 0.02–0.04 whereas the quantum defects for the f waves attached to the $(4s3d)^1D$ threshold are ~ 0.07–0.10. This means the $(4s3d)^1Dnf$ states are more deeply bound (compared to their threshold) than the $(3d^2)^3Fnf$ states. This trend arises from the difference in the size of the $4s$ and $3d$ orbitals (see Fig. 1 of Ref. [1]). The $4s$ orbital is larger than the $3d$ orbital and therefore does not screen the nuclear charge as effectively; the $4s$ state is also more easily

polarized. These two effects ensure that the electron-Sc$^+$ interaction is more attractive when the Sc$^+$ has a $(4s3d)^1D$ core than when it has a $(3d^2)^3F$ core.

V. CONCLUSIONS

We have obtained the experimental photoionization spectrum from threshold to just above the $(3d^2)^3F$ thresholds (a range of ~ 0.6 eV). We have compared the predicted theoretical spectrum to the experiment and found very good agreement between the two. We have listed the positions and classifications of several new autoionizing lines and compared them with the previous levels of Garton et al. [3] where possible. We have also compared the ground-state cross section to that from the excited state which illustrates the role played by the dipole operator; this suggests the desirability for obtaining the cross section from different initial states whenever possible as an aid in the interpretation of spectra.

The experimental results presented here provide an extensive measurement of excited state photoionization of Sc suitable for a comprehensive test of theory. A relatively simple application of standard spectroscopic techniques indicates the feasibility of further experimental studies of photoionization in the transition metals. In addition, use of an atomic beam rather than the high temperature vapor of earlier photoabsorption work allowed measurements at much higher resolution. For example, the Doppler width of the Sc vapor (~ 20 Ghz at $\lambda = 500$ nm) in the work of Garton et al. [3] exceeded our ~ 0.5 cm^{-1} linewidth. Photoionization measurements in transition metals other than Sc would typically require much higher temperatures, so the Doppler width of a vapor could impose serious limitations to experimental resolution. The simple and relatively inexpensive experimental methods demonstrated in this work, coupled with continuing improvements in the theory, should illustrate the viability of further studies of the transition metals.

The comparison of theory with experiment in this series indicates the level of accuracy that can be achieved with the eigenchannel R matrix and MQDT (with frame transformations); it shows that a moderate effort can result in spectra useful on a global and line-by-line scale. The Sc spectra are extremely complex due to the large number of closely spaced thresholds; the fact that its dynamics could be unraveled bodes well for future efforts. The level of accuracy achieved indicates a high probability for a successful theoretical characterization of the heavier transition metals which can have more importance for other areas of physics. In this presentation we have tried to go beyond a bare presentation of results and wherever possible we have tried to give microscopic and global reasons for the appearance of the spectra. We are not solely interested in calculating spectra to show that it can be done; we have explored the reasons for the success and once it was obtained explored the details of the atomic dynamics. We expect that many of the lessons learned for Sc will apply to the other transition metals and we hope that this expected similarity can soon be traced.

ACKNOWLEDGMENTS

* Present address: Department of Physics, Auburn University, Auburn, AL 36849-5311.

[1] F. Robicheaux and C.H. Greene, this issue, Phys. Rev. A **48**, 4429 (1993).

[2] F. Robicheaux and C.H. Greene, Phys. Rev. A **48**, 4441 (1993).

[3] W.R.S. Garton, E.M. Reeves, F.S. Tomkins, and B. Ercoli, Proc. R. Soc. London, Ser. A **333**, 1 (1973).

[4] J. Sugar and C. Corliss, J. Phys. Chem. Ref. Data **14**, Suppl. No. 2 (1985).

[5] D.J. Armstrong, R.P. Wood, and C.H. Greene, Phys. Rev. A **47**, 1981 (1993).

[6] W.E. Cooke, S.A. Bhatti, and C.L. Cromer, Opt. Lett. **7**, 69 (1982).

[7] S.A. Bhatti and W.E. Cooke, Phys. Rev. A **28**, 756 (1983).

[8] S. Gerstenkorn and P. Luc, Laboratorie AIME-Cotton CNRS II report, Orsay (France) (unpublished).

[9] R. E. Honig and D. A. Kramer, RCA Rev. **30**, 285 (1969).

[10] F.S. Tomkins and B. Ercoli, Appl. Opt. **6**, 1299 (1967).

[11] F. Robicheaux and C.H. Greene, Phys. Rev. A **46**, 3821 (1992); *ibid.* **47**, 1066 (1993).

[12] C.H. Greene and L. Kim, Phys. Rev. A **38**, 5953 (1988).

[13] A.R.P. Rau and U. Fano, Phys. Rev. A **4**, 1751 (1971); C.M. Lee and K.T. Lu, *ibid.* **8**, 1241 (1973).

[14] U. Fano and A.R.P. Rau, *Atomic Collisions and Spectra* (Academic, Orlando, 1986); M.J. Seaton, Rep. Prog. Phys. **46**, 167 (1983).